# Ferroelectricity and structure of BaTiO$_3$ grown on YBa$_2$Cu$_3$O$_{7-\delta}$ thin films

Ch. Schwan, F. Martin, G. Jakob, J.C. Martinez[a], and H. Adrian

Institut für Physik, Johannes Gutenberg-Universität Mainz, 55099 Mainz, Germany

**Abstract.** We have investigated the crystal structure and the ferroelectric properties of BaTiO$_3$ thin films with YBa$_2$Cu$_3$O$_{7-\delta}$ as the bottom and Au as the top electrode. Epitaxial heterostructures of YBa$_2$Cu$_3$O$_{7-\delta}$ and BaTiO$_3$ were prepared by dc and rf sputtering, respectively. The crystal structure of the films was characterised by X-ray diffraction. The ferroelectric behaviour of the BaTiO$_3$ films was confirmed by hysteresis loop measurements using a Sawyer Tower circuit. We obtain a coercive field of 30 kV/cm and a remanent polarisation of 1.25 $\mu$C/cm$^2$. At sub-switching fields the capacitance of the films obeys a relation analogous to the Rayleigh law. This behaviour indicates an interaction of domain walls with randomly distributed pinning centres. At a field of 5 MV/m we calculate a 3% contribution of the irreversible domain wall motion to the total dielectric constant.

**PACS.** 74.76.-w Superconducting films – 77.55.+f Dielectric thin films – 77.80.-e Ferroelectricity and antiferroelectricity

## 1 Introduction

In recent years, there has been much interest in the preparation of superconducting field effect transistors (SuFETs) with a (Ba,Sr)TiO$_3$ thin film as gate insulator and YBa$_2$Cu$_3$O$_{7-\delta}$ (YBCO) as source-drain channel [1]. More recently the development of high frequency superconducting devices increased the interest of the community in YBCO/ferroelectric heterostructures [2]. From these studies it became clear that it is possible to grow high quality perovskite ferroelectric thin films on top of YBCO electrodes. This motivated us to investigate the room temperature ferroelectric and structural properties of YBCO/BaTiO$_3$/Au heterostructures.

The objective of this work is to analyse the domain wall contribution to the dielectric properties of high quality BaTiO$_3$ (BTO) thin films. So far, similar studies have only been done on Pt/PbZr$_x$Ti$_{1-x}$O$_3$ (PZT)/Pt heterostructures [3].

## 2 Experiment

The 100 nm thick YBCO layers and the BTO films were sputtered *in situ* in pure O$_2$ atmosphere. The top Au electrodes were thermally evaporated through a shadow mask. Before deposition, the YBCO target was pre-sputtered for 1 hour and the BTO target for 30 minutes. After this time the dc-voltage of the plasma did not decrease anymore showing that the targets reached a stable state. For

both processes the substrate target distance was about 20 mm. The heterostructures have been prepared on MgO substrates because of the better high frequency properties of this material in comparison to SrTiO$_3$. The YBCO ground electrode was prepared following the method already described in detail in reference [4]. The difference in the present work is that the post annealing was performed after the deposition of the BTO layer. The stoichiometric BTO targets were prepared at the University of Mainz. The BTO films were deposited by rf-sputtering in an on-axis geometry without a magnetron, in O$_2$ pressures between 0.5 and 1.5 mbar. This was needed in order to prevent re-sputtering. During deposition, the rf power was regulated at 130 W resulting in a typical bias voltage of 30 V. The best films were deposited at 700 °C. At the end of the process, the bi-layers were cooled down to room temperature during 1 hour and annealed in 1 bar oxygen pressure. The electrode contact size varied between 0.5 mm$^2$ and 1 mm$^2$. X-ray diffraction patterns in Bragg-Brentano and four-circle geometry were obtained using a Philips X'Pert-MPD and a STOE STADI4 diffractometer, respectively. The capacitance and the hysteresis loops were measured with a HP4284A LCR-meter and a self made Sawyer-Tower circuit, respectively.
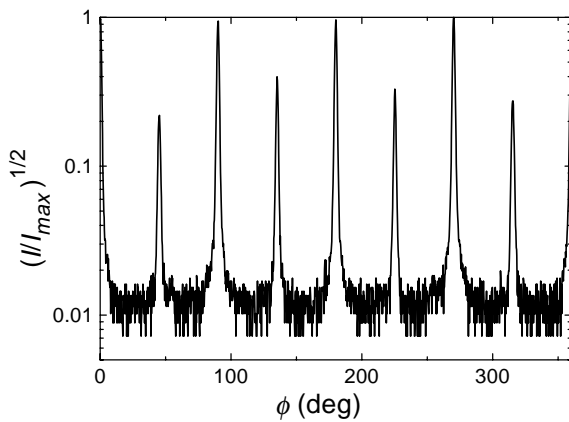
## 3 Results and discussion

### 3.1 X-ray diffraction

The $\theta/2\theta$-scan shown in Figure 1 reveals only $c$-axis oriented growth of the BTO films. However as shown by
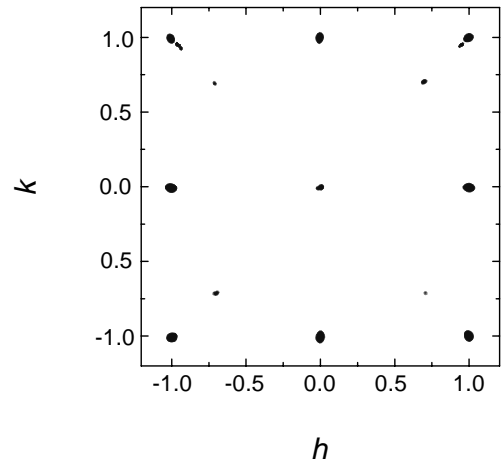
[a] e-mail: `martinez@mail.uni-mainz.de`
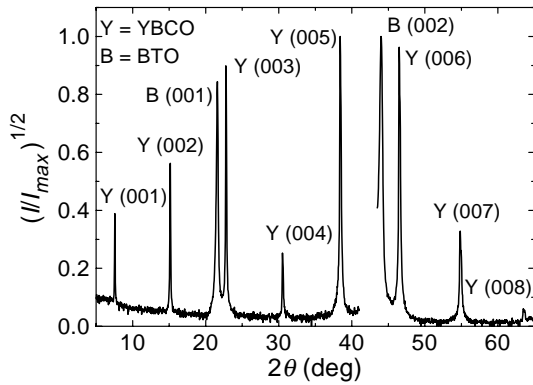
**Fig. 1.** $\theta/2\theta$ scan of YBCO/BTO. Both YBCO and BTO show $c$-axis oriented growth. The YBCO peaks are labelled with a Y and the BTO peaks with a B.



**Fig. 2.** $\phi$ scan of the YBCO (103) reflection. There are 8 peaks indicating the alignment of YBCO parallel and 45° rotated to the MgO substrate. Both orientations exhibit a fourfold symmetry.



**Fig. 3.** Two-dimensional scan of the plane $\ell = 1$ for BTO. The 8 reflexes are caused by the epitaxial growth of BTO on top of YBCO.
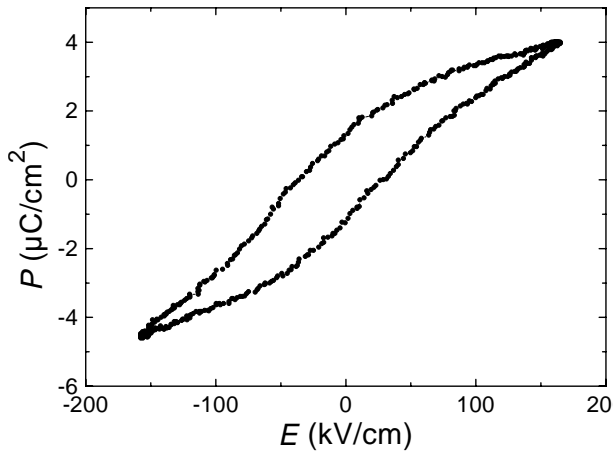
there are 8 peaks, indicating a fourfold symmetry and an in-plane alignment of the YBCO's and BTO's crystallographic axes parallel and rotated 45° relative to the MgO lattice. The rotated alignment can be explained by the fact that 2 lattice constants of MgO equals 3 diagonal lattice parameters of YBCO. Since BTO grows on YBCO epitaxially it reproduces this 45° rotation.

A fourfold symmetry was obtained by the use of $SrTiO_3$ substrates. The orientation matrix gives for our films the in-plane lattice constants $a = b = (0.3994 \pm 0.0002)$ nm for BTO. This value is in excellent agreement with the result from bulk materials. For YBCO we measured $a = 0.3847$ nm, $b = 0.3851$ nm. These values coincide well with the average between $a$ and $b$ in bulk materials. This is due to the usual mixing of these two orientations observed in thin films done on standard substrates. The results above show that the $c$-axis distortion of BTO cannot be explained by the requirement to conserve the unit cell volume, according to the Poisson ratio. This indicates that the high energy of barium at the sputtering process might be indeed responsible for the observed lattice distortion.

The mosaic spreads of the different layers were determined by measuring the rocking curves of BTO (002) and YBCO (005). For BTO we obtain a FWHM (full width at half maximum) of 0.38° and for YBCO 0.32°, indicating a good epitaxial growth of the heterostructures. The small FWHM obtained in our BTO films can be explained by a reduced lattice mismatch between YBCO and BTO. For comparison, Wills *et al.* obtained for $a$-axis oriented BTO on $LaAlO_3$ substrates a FWHM of 0.6° [8].

## 3.2 Ferroelectric hysteresis loops

The non-remanent component of polarisation is caused by non-ferroelectric ionic and electronic polarisability as well as field induced reversible ferroelectric domain wall motion. The remanent component is induced

detailed TEM studies, there may still exist small amounts of $a$-axis oriented domains embedded on a $c$-axis matrix even if by X-ray diffraction no splitting caused by $a$-and $c$-axis oriented domains can be found [5]. The $c$-axis length of the BTO thin films in our work sputtered at 0.7 mbar is determined to be 3% larger in comparison with the bulk material and coincides with the value obtained in the work of Abe *et al.* [6]. On the other hand, by using a deposition pressure of 1.5 mbar we obtain the same $c$-axis length as the bulk material. Hence the lattice expansion at a lower pressure may result from atomic defects due to the high kinetic energy of the incident species. This explanation is in accordance with our observation that the lattice expansion occurs only for BTO but not for $SrTiO_3$ thin films. As barium ions are much heavier than strontium ions they can induce more serious damage upon impact on the previously deposited film. We expect therefore the lattice parameters to be also dependent on the deposition technique, as already reported by Srikant *et al.* [7].

In order to characterise the in-plane orientation of the YBCO/BTO heterostructures we performed a $\phi$-scan of the YBCO (103) reflex (see Fig. 2) and a two-dimensional scan of the plane $\ell = 1$ for BTO (see Fig. 3). For both films

**Fig. 4.** Polarisation *vs.* field hysteresis loop. Using a Sawyer-Tower circuit, we obtain a remanent polarisation of $P_r = 1.25 \ \mu\text{C/cm}^2$ and a coercive field of $E_c = 30$ kV/cm.



**Fig. 5.** Field dependence of the capacitance at different frequencies. The full lines represent the fits according to the Rayleigh law.



**Fig. 6.** Frequency dependence of the capacitance. The full lines represent logarithmic fits.

by the switching of ferroelectric domains. Using a Sawyer-Tower circuit, we obtain a remanent polarisation of $P_r = 1.25 \ \mu\text{C/cm}^2$ and a coercive field of $E_c = 30$ kV/cm (Fig. 4). These results are consistent with measurements done by other groups on BTO thin films deposited by rf-sputtering [9,10] and Pulsed Laser Deposition [11,12]. Measurements of the dielectric constant of our 300 nm thick BTO films, from room temperature to 200 °C, did not indicate any sign of a ferroelectric phase transition. This is in agreement with the data of Yoneda *et al.*, which observed for 30 mono-layers thick BTO films a ferroelectric hysteresis up to 600 °C [13]. These results are rather surprising since bulk BTO is known to have a Curie temperature of about 120 °C and much larger remanent polarisation [14,15]. However, we think that these discrepancies in the ferroelectric properties are due to the lattice distortions observed in thin films.

## 3.3 Contribution of the domain walls to the permittivity

The major research in ferroelectric thin films emphasises the nucleation, growth and switching of domains because these features are very important for nonvolatile memory applications. In contrast, contributions to the dielectric or the piezoelectric constant at sub-switching fields due to domain wall displacements and vibrations were investigated mainly for single crystals or ceramics. We follow here the procedure of Taylor *et al.* by extending the models for the interaction and pinning of domain walls with randomly distributed pinning centres in magnetic materials, to the dielectric displacement in ferroelectric thin films [3]. Below we will address the dielectric response of a BTO thin film both in terms of the weak-field (Rayleigh law) and the logarithmic frequency dependence. The Rayleigh law is valid for low-field conditions, where no nucleation of domains occurs and the average structure of the domain walls drifts within the sample as the field is cycled [16]. In order to achieve the linear Rayleigh behaviour for the
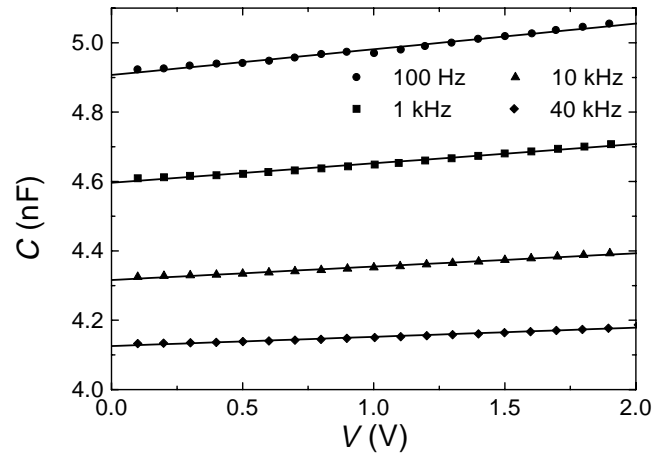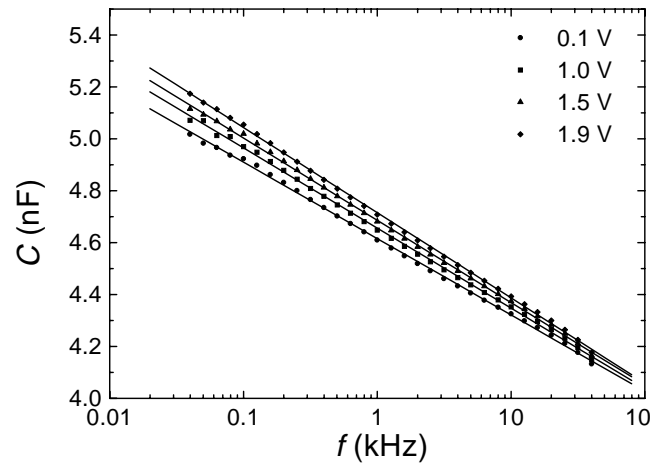
dielectric constant we cycled the sample about $10^7$ times prior to the measurement with an amplitude below the coercive voltage. Figure 5 shows the linear dependence of the capacitance versus ac voltage amplitude $V_0$. From the capacitance at 100 Hz, and from the geometry of our electrodes we deduce a dielectric constant $\epsilon = 300$. In accordance to the Rayleigh law the weak-field dependence can be described by the formula $C = C_{\text{init}} + aV_0$. $C_{\text{init}}$ represents the intrinsic lattice and reversible domain wall movement. The second term $aV_0$ with the Rayleigh coefficient $a$ is responsible for the weak-field hysteresis due to the pinning and depinning of domain walls. According to Néel it is caused by the irreversible displacement of the walls between two meta-stable states when the applied field is large enough to overcome the barrier. In Figure 6 we show the logarithmic dependence of the capacitance on frequency. As for magnetic systems this logarithmic behaviour is generally attributed to domain wall motion across randomly distributed pinning centres [3,17]. In
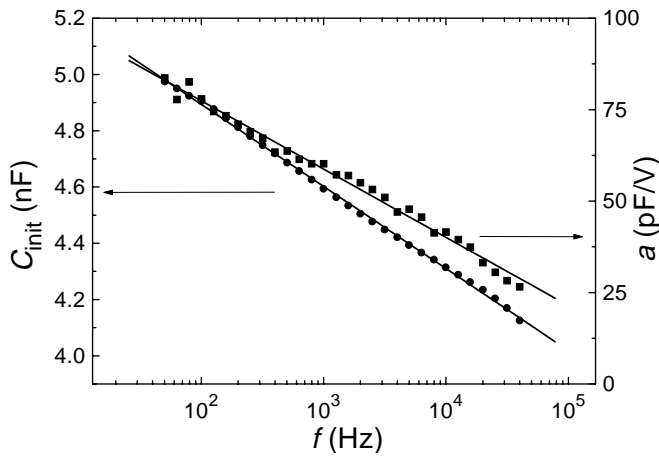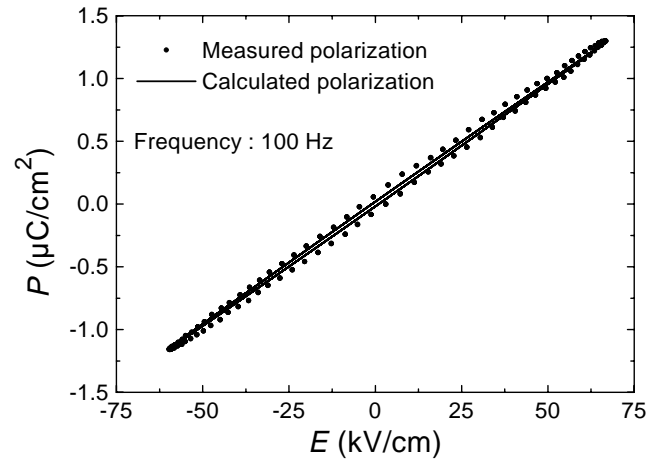
**Fig. 7.** Frequency dependence of the reversible and irreversible parameters $C_{\text{init}}$ and $a$ of the capacitance.



**Fig. 8.** $P(E)$ hysteresis loop for $E_0 = 2$ MV/cm at 100 Hz. Circles correspond to experimental data and the full lines are calculated with $C_{\text{init}}$ and $a$ extracted from Figure 5.

order to determine whether the reversible $C_{\text{init}}$ or the irreversible Rayleigh coefficient $a$ is responsible for this behaviour, we extracted them for all frequencies from the ac field dependence of the capacitance. The result indicating the logarithmic frequency dependence of both parameters is presented in Figure 7. Using a Sawyer-Tower circuit we finally measured the non-saturating hysteresis loop (Rayleigh loop) of our samples at sub-switching fields (see Fig. 8). The full line representing the calculated hysteresis curve is based on the LCR-meter measurement by using the formula $P = (\epsilon_{\text{init}} + \alpha E_0)E \pm \alpha/2(E_0^2 - E^2)$, where $+$ stands for the decreasing and $-$ for the increasing field. $\epsilon_{\text{init}}$ and $\alpha$ are derived from $C_{\text{init}}$ and $a$ respectively. $E_0$ designates the maximum field reached during the cycle. While the slopes of the loops coincide, the area of the calculated hysteresis curve is underestimated in comparison to the measured one. This fact suggests that the observed hysteresis is not only due to the Rayleigh-type irreversible contribution of the dielectric constant, but by the losses having their origin in the series resistance and parallel conductivity of the capacitor. This explanation is confirmed by the fact that the calculated curve is only based on the imaginary and not on the real part of the impedance.

So far there is no universal behaviour for the frequency response of capacitors based on insulating perovskites. While Taylor $et$ $al.$ observed, for Pt/PZT/Pt capacitors, in the range from $10^{-1}$ Hz to $10^4$ Hz an exponential law between capacitance and frequency [3], Zafar $et$ $al.$ used for Pt/(Ba,Sr)TiO$_3$/Pt between $10^2$ Hz and $10^6$ Hz a power law to describe their data [18].

While the logarithmic frequency dependence is in accordance with the contribution of domain walls, the power law dependence is known as the Curie-von Schweidler law. Obviously further studies are necessary to determine the correct relationship between the dielectric constant and the frequency. Maybe our data and the results of Taylor $et$ $al.$, fit better to the logarithmic frequency dependence because the films exhibit a remanent polarisation and thus a higher domain wall contribution in comparison to non-ferroelectric (Ba,Sr)TiO$_3$ films. The relative irre-

versible domain wall contribution to the total capacitance can be obtained by the ratio $aV/C$. If we apply a sinusoidal electrical field with a frequency of 100 Hz and an amplitude of $E_0 = 5$ MV/cm we obtain a ratio of 3%. This value is much smaller than the 21% calculated by Taylor $et$ $al.$ for 1.3 $\mu$m thick PZT thin films. Since the irreversible part of the dielectric constant determines the remanent polarisation it is reasonable for BTO to obtain a lower contribution of irreversible domain wall movement than for PZT because the remanent polarisation of PZT thin films is typically in the range of 40 $\mu$C/cm$^2$. This is more than one magnitude larger in comparison with our BTO thin films (1.25 $\mu$C/cm$^2$).

The grain size and the stresses due to the phase transition determine the dielectric constant in ceramics. But ferroelectric thin films are additionally influenced by the existence of interfaces and additional stresses, caused by the lattice mismatch between film and substrate.

## 4 Conclusion

The small lattice mismatch and chemical compatibility between YBCO and BTO allow a good crystal structure for heterostructures of both materials. X-ray diffraction patterns display a high degree of crystalline order of both YBCO and BTO, whereas their in-plane orientation is influenced by the choice of MgO as substrate material. The sub-switching ac electric field dependence of the permittivity may be described in terms of the Rayleigh law. At a field of 5 MV/m the total dielectric constant contains a contribution of 3% from the irreversible domain wall movement. In addition to $C_{\text{init}}$ the irreversible Rayleigh parameter representing irreversible domain wall movement shows also a linear logarithmic frequency dependence of permittivity. This behaviour can be explained by pinning of domain walls. In comparison to conventional Pt as base electrode for ferroelectric memories, YBCO offers the advantages of better fatigue behaviour.

## References

1. J. Mannhart, Supercond. Sci. Technol. **9**, 49 (1996).
2. F. Jin, G.W. Auner, R. Naik, N.W. Schubring, J.V. Mantese, A.B. Catalan, A.L. Micheli, Appl. Phys. Lett. **73**, 2838 (1998).
3. D.V. Taylor, D. Damjanovic, J. Appl. Phys. **82**, 1973 (1997).
4. M. Schmitt, S. Freisem, T. Becherer, A. Hadish, H. Adrian, J. Appl. Phys. **76**, 3220 (1994).
5. S. Kim, S. Hishita, Y.M. Kang, S. Baik, J. Appl. Phys. **78**, 5604 (1995).
6. K. Abe, S. Komatsu, J. Appl. Phys. **77**, 6461 (1995).
7. V. Srikant, E.J. Tarsa, D.R. Clarke, J.S. Speck, J. Appl. Phys. **77**, 1517 (1995).
8. L.A. Wills, B.W. Wessels, Appl. Phys. Lett. **60**, 41 (1992).
9. M.H. Song, Y.H. Lee, T.S. Hahn, M.H. Oh, K.H. Yoon, J. Appl. Phys. **79**, 3744 (1996).
10. H.-F. Cheng, J. Appl. Phys. **79**, 7965 (1996).
11. K. Kaemer, H. Huetz, B. Holzaofel, W. Haessler, L. Schultz, J. Phys. D **30**, 522 (1997).
12. H.S. Wang, Y.W. Liu, K. Ma, Z.Q. Peng, D.F. Cui, H.B. Lu, Y.L. Zhou, Z.H. Chen, L. Li, G.Z. Wang, Physica C **282**, 699 (1997).
13. Y. Yoneda, T. Okabe, K. Sakaue, H. Terauchi, J. Appl. Phys. **83**, 2458 (1998).
14. F. Jona, G. Shirane, *Ferroelectric Crystals* (Pergamon, New York, 1962), p. 389.
15. Ch. Kittel, *Introduction to Solid State Physics*, 6th edn. (John Wiley & Sons, Inc. New York, 1996), p. 396.
16. D. Damjanovic, J. Appl. Phys. **82**, 1788 (1997).
17. T. Natterman, Y. Sapir, I. Vilfan, Phys. Rev. B **42**, 8577 (1990).
18. S. Zafar, R.E. Jones, P. Chu, B. White, B. Jiang, D. Taylor, P. Zurcher, S. Gillespie, Appl. Phys. Lett. **72**, 2820 (1998).
19. G. Arlt, D. Hennings, G. de With, J. Appl. Phys. **58**, 1619 (1985).